THE JOURNAL OF PHYSICAL CHEMISTRY C

ARTICLE

pubs.acs.org/JPCC

# Steady-State Statistical Sputtering Model for Extracting Depth Profiles from Molecular Dynamics Simulations of Dynamic SIMS

Robert J. Paruch,[†] Zbigniew Postawa,[†] Andreas Wucher,[‡] and Barbara J. Garrison[§,*]

[†]Smoluchowski Institute of Physics, Jagiellonian University, Ulica Reymonta 4, 30-059 Kraków, Poland

[‡]Faculty of Physics, University of Duisburg-Essen, 47048 Duisburg, Germany

[§]Department of Chemistry, 104 Chemistry Building, Penn State University, University Park, Pennsylvania 16802, United States

**ABSTRACT:** Recently a "divide and conquer" approach was developed to model by molecular dynamics (MD) simulations dynamic secondary ion mass spectrometry (SIMS) experiments in order to understand the important factors for depth profiling. Although root-mean-square (rms) roughness can be directly calculated from the simulations, calculating depth profiles is beyond the current capability of the MD simulations. The statistical sputtering model (SSM) of Krantzman and Wucher establishes the foundation for connecting information from the MD simulations to depth profiles. In this study, we revise the SSM to incorporate more extensive information from the MD simulations in the steady-state region, thus presenting the steady-state statistical sputtering model (SS-SSM). The revised model is utilized to interpret MD simulations of 20 keV $C_{60}$ bombardment of Ag at normal incidence as well as the effect of sample rotation on depth profiling.

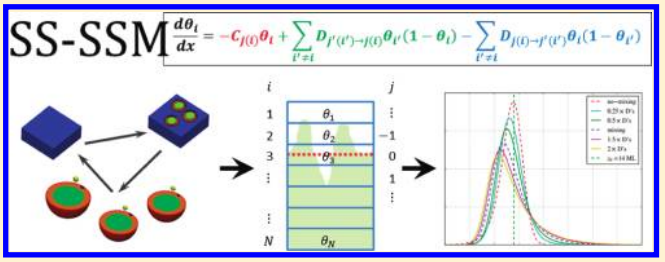


## INTRODUCTION

The development of cluster beam sources for secondary ion mass spectrometry (SIMS) and the realization that they can be used for molecular depth profiling[1] has stimulated the interest in finding a way of converting the information obtained from simulations of individual impacts of the clusters into the actual depth profiles. Modeling of single impacts by molecular dynamics (MD) simulations requires a modest sized sample of several hundred thousand particles. Modeling of depth profiling, that is, dynamic SIMS, increases the size of the sample by at least an order of magnitude. Consequently, modeling even a single impact on the large sample requires a very long time to complete. In addition, as hundreds to thousands of sequential impacts are needed to calculate depth profiles, the simulations could last for years. Recently, however, a "divide and conquer" approach was developed to make dynamic SIMS MD simulations possible.[2] It is now feasible to model up to fluences approaching $10^{14}$ impacts/cm$^2$ in several months of computer time.[3−6] The amount of material removed with these heroic calculations, however, is still only less than a handful of monolayer equivalents, which is far from the amount of material removed in a typical depth profiling experiment. Thus, it is not possible to extract a depth profile or an interface width, key experimental metrics of depth profiling quality. The issue is how to take the wealth of simulation data that should contain all the physics relevant for the depth profile and create the appropriate depth profile.

Krantzman and Wucher have developed a statistical sputtering model (SSM) to investigate the evolution of an eroded system toward equilibrium by using data from the initial stages of a MD simulation.[6] This model evaluates the occupation of each layer in the system as a function of the amount of removed material; thus, extracting depth profiles is straightforward. The input quantities to the model come from the MD simulations that contain the properties of the target material, the incident cluster and the initial beam conditions. Thus, the SSM is ideal to connect the plethora of data obtained in the MD simulations[3−5] to depth profiles.

In this paper, we present a revised SSM model in which the data for the model are obtained from the steady-state region of the dynamics SIMS MD simulation rather than from the beginning of the erosion process. It is our belief that the microscopic details of the bombarded surface are sufficiently different from the flat surface that it is important to use input from the steady-state region to describe the depth profile. Specifically, with a roughened surface, the range of depths from which atoms can sputter is larger and displacements of atoms can occur over a greater depth range. The model is applied to interpret simulation results obtained from dynamic SIMS MD simulations of bombardment of Ag(111) by 20 keV $C_{60}$ at normal incidence. In particular, the effects of the sputtering information depth and the interlayer mixing on the shape of the depth profiles are discussed. The model is also used to interpret results of two depth-profiling experiments.

## STEADY-STATE STATISTICAL SPUTTERING MODEL

Krantzman and Wucher proposed the SSM to determine depth profiles from a MD simulation of dynamic SIMS for a target

**Received:** October 12, 2011
**Revised:** November 23, 2011
**Published:** December 03, 2011

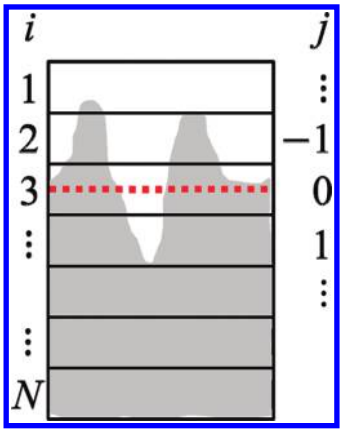


**Figure 1.** Schematic of the system divided into layers with two index schemes, *i* and *j*, and the roughened sample surface. The red dotted line denotes the average surface level, $i_{av} = 3$. The connection between *i* and *j* is $j = i - i_{av}$.

of Si.[6] Their model is expressed by a set of differential equations for the filling factor or fractional population in each layer of the system. Changes in the filling factor occur due to sputtering and material relocation between adjacent layers, which is characterized by Fick's first law of diffusion. The sputtering and diffusion coefficients are determined from the MD simulation data for the initial few impacts. The solution of the differential equations leads to depth profiles. Their primary interest was to take the low-dose MD simulations and examine the evolution of the depth profiles to the steady-state conditions, where the characteristics of the depth profiles are distinctive for the simulated system.

Our interest in the SSM model is to use it to connect the microscopic information obtained from the simulations, such as the information depth of sputtering and the interlayer displacements, to interpret the depth profiles as a function of beam conditions. Accordingly, several modifications have been made to the original SSM model. (1) The parameters are extracted from the steady-state region of the MD simulation; thus, this version of the model is the steady-state SSM (SS-SSM). Using data from a roughened surface broadens the distributions of the sputtering and displacement quantities. (2) Material relocation is described by the number of displaced particles between all pairs of layers rather than by Fick's law of diffusion coefficients that only connect adjacent layers. This description is conceptually well connected to the MD simulations from which this information is determined. As a result, the differential equations include displacement contributions, $D_{j\rightarrow j'}$, between all pairs of layers. From the point of view of the model, the exact nature of these relocations is unimportant. In this study, we consider ion-induced mixing. (3) The statistical approach for defining layer contributions to sputtering and mixing is replaced with a reference level that corresponds to the average surface level. The system properties such as sputtering and displacement are defined relative to the reference level.

The system is described by layers as shown in Figure 1. The main labeling scheme is the space fixed one with the index *i*, where *i* goes from 1 to *N*, and *N* denotes the number of system layers. The differential equations presented in subsequent text give the filling factor for each of these layers as a function of the amount of eroded material. The *j* indices label layers relative to the average surface level, $i_{av}$, which in Figure 1 has a value of 3. The layer $j = 0$ corresponds to the layer that is approximately half-occupied, which is considered as the average surface level. The value of $i_{av}$ changes as the system is eroded. The sputtering and displacement coefficients described below are defined with respect to the position of the particular layer relative to the average surface level; that is, they are described by the *j*-index.

As suggested by Krantzman and Wucher,[6] the natural variable for the model is *x*, the number of monolayer equivalents removed from the system, and $\theta_i$, the filling factor of the *i*th layer. The filling factor is defined as

$$\theta_i = \frac{n_i}{N_{atoms}} \tag{1}$$

where $n_i$ is the current number of atoms in the *i*th layer and $N_{atoms}$ is the number of atoms in a totally filled layer. The range of values of $\theta_i$ extends from zero for a completely empty layer to unity for a completely filled layer. The modified differential equations for the SS-SSM are as follows:

$$\frac{d\theta_i}{dx} = -C_j\theta_i - \sum_{i'\neq i} D_{j\rightarrow j'}\theta_i(1-\theta_{i'}) + \sum_{i'\neq i} D_{j'\rightarrow j}\theta_{i'}(1-\theta_i) \tag{2}$$

where $i$, $i'$ go from 1 to $N$, $j = i - i_{av}$, and $j' = i' - i_{av}$ as shown schematically in Figure 1. The interpretation of the terms is straightforward. For each layer *i*, there can be loss of particles by sputtering or displacements to other layers and there can be a gain of particles by displacements from other layers. The sputtering term is a product of the sputtering coefficient per layer, $C_j$, times the filling factor $\theta_i$. Each displacement term is a product of the displacement coefficient between two layers, $D_{j\rightarrow j'}$, times the filling factor $\theta_i$ for the initial layer and the vacancy factor $(1 - \theta_{i'})$ for the final layer. The average surface level, that is, the value of $i_{av}$, switches when the accumulation of the quantity $(Y/N_{atoms})\Sigma_i C_j\theta_i$ over a number of consecutive integration steps for all system layers equals 1, which indicates the removal of one monolayer equivalent from the system. The quantity *Y* is the total sputtering yield. The prescription of how to collect the parameters, including the initial filling factors, the sputtering $(C_j)$ and displacement $(D_{j\rightarrow j'})$ coefficients, is described in the next section.

**Collecting Data from the Simulation.** The root-mean-square (rms) roughness and average surface level as a function of fluence from a simulation[3,4] of 20 keV $C_{60}$ bombardment of a Ag(111) surface are shown in Figure 2. The details of the calculation of the average surface level and rms roughness have been previously given in detail.[2,3] Briefly, the surface is discretized into columns. The average surface level is the mean of the highest atom position in each column, and the rms roughness is the root-mean-square deviation of the highest atom position relative to the average surface level. The simulation starts with a perfectly flat surface; thus, there is an induction period before the steady-state region where the rms roughness is relatively constant and the average surface level recedes at a constant rate. For evaluating the initial filling factors, sputtering and displacement coefficients, only impacts in the steady-state region are used. The advantage of such an approach is that all of these coefficients will not depend on the fluence. They are calculated as an average over 1000 impacts by the following procedure. First, the beginning of a steady-state region is identified. Next, atoms are binned into appropriate system layers labeled by index *i*. From the point of view of the model, the system layers do

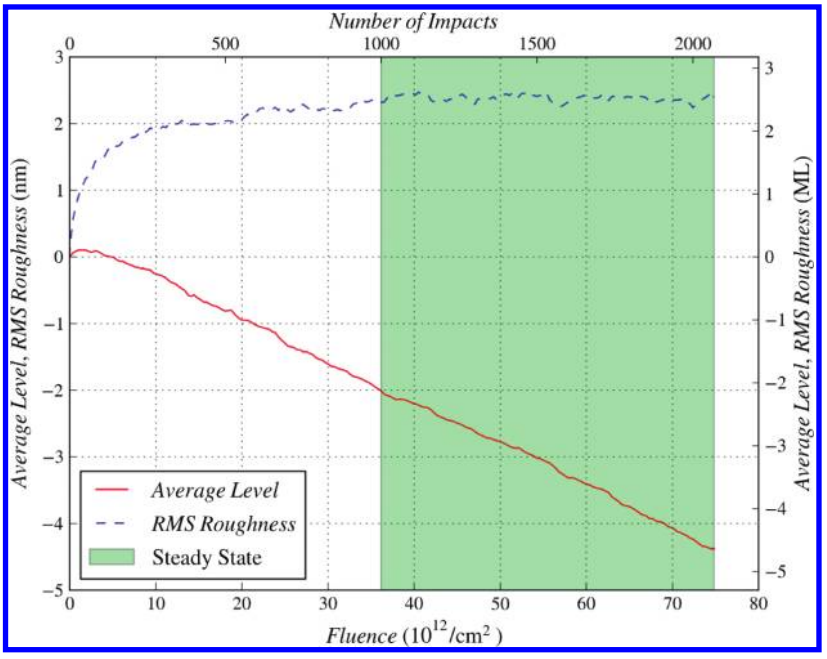


**Figure 2.** Average surface level and rms roughness vs fluence from the "divide and conquer" MD simulation. The incident particle is $C_{60}$ at 20 keV incident energy bombarding normal to the Ag(111) surface. The green shading denotes the steady-state region.

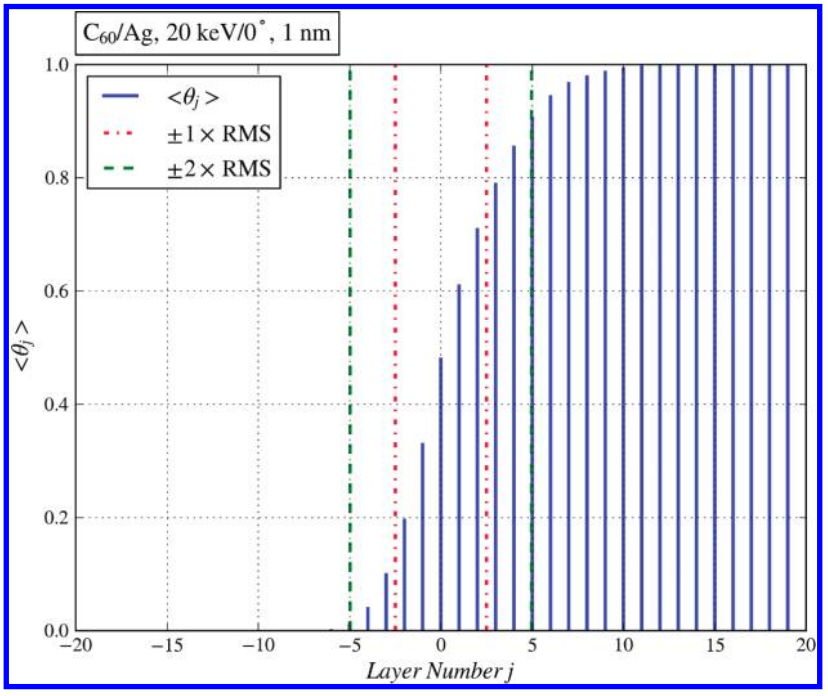


**Figure 3.** Average filling factor, $\langle\theta_j\rangle$, vs layer number, $j$. The red and green vertical lines correspond to $\pm1$ and $\pm2$ × rms roughness positions, respectively.

not have to be identical with atomic layers of a probed crystal. In fact, we have selected layers with a thickness of 0.94 nm, which corresponds to four atomic layers of the Ag(111) crystal. Selection of layers larger than atomic spacings makes the model results more easily comparable to experimental measurements. The influence of the layer size on the results is discussed in the next section. After binning, the average surface level is determined and all the particles are assigned to the appropriate $j$-layer and all parameters required to solve eq 2 are calculated. The above steps are repeated for each impact. Finally, the averaged values are calculated for the quantities of interest.

The average filling factor $\langle\theta_j\rangle$ as shown in Figure 3 is an average over all impacts within the steady-state region. For each impact, the average surface level is determined to assign the $j = 0$ layer. The vertical lines show the positions of $\pm1$ and $\pm2$ × rms roughness values relative to the average surface layer ($j = 0$), and it is clear that most of the change in the filling factor is in this region. To determine the sputtering and displacement coefficients,


dx.doi.org/10.1021/jp2098075 |J. Phys. Chem. C 2012, 116, 1042–1051

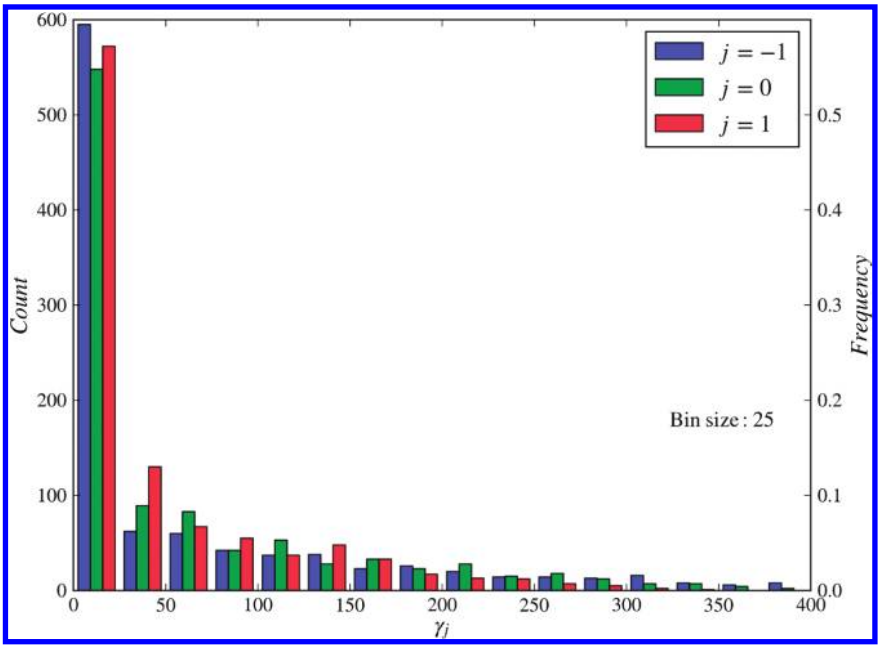


**Figure 4.** Histogram of the frequency of individual sputtering yields for $j = 0, \pm 1$.

the layer locations of the system particles before and after an impact are used. Starting with the sputtering terms, the individual sputtering yields, $\gamma_k^j$, for each impact $k$ are evaluated. A histogram giving the frequency of each yield is shown in Figure 4 for $j = 0$, $\pm 1$. The average sputtering yield for layer $j$, $\Gamma_j$, is the average of the individual sputtering yields and is given by

$$\Gamma_j = \frac{1}{K} \sum_k \gamma_k^j \tag{3}$$

where $k = 1, 2, 3, ..., K$ and $K$ denotes the number of impacts within the steady-state region. There is tremendous scatter in the individual $\gamma_k^j$ quantities due to the surface topography. As shown schematically in Figure 1, the surface is very corrugated. The individual sputtering yield will depend on the point of impact. For instance, the sputtering yield is different if the projectile impacts at the hill or in the valley.[2] For this model, however, we only consider the average values, $\Gamma_j$, as shown in Figure 5. The largest sputtering yield for this set of beam conditions is from the $j = -1$ layer which is above the average surface level. The width of the sputtering distribution is comparable to the average surface level $\pm 2 \times$ rms roughness distance, which indicates that most of the sputtered particles come from the exposed surface. To determine the $C_j$ coefficients needed in the differential equation, one must first calculate the total sputtering yield, $Y$, as given by

$$Y = \sum_j \Gamma_j \tag{4}$$

Now, the coefficients $C_j$ can be expressed as

$$C_j = \begin{cases} 0 & \text{for } \langle\theta_j\rangle = 0 \\ \dfrac{\Gamma_j}{Y\langle\theta_j\rangle} & \text{for } \langle\theta_j\rangle \neq 0 \end{cases} \tag{5}$$

This definition is consistent with the original reference except that in this reference the initial system had only empty or completely filled layers. In the original representation, the definition of $C_j$, therefore, does not need $\langle\theta_j\rangle$ in the denominator of eq 5.[6] By definition,

$$\sum_j C_j\langle\theta_j\rangle = 1 \tag{6}$$

In a similar manner, the number of atoms displaced from layer $j$ to layer $j'$, $\Delta_{j\to j'}$, and the displacement coefficient, $D_{j\to j'}$, are calculated as follows:

$$D_{j\to j'} = \begin{cases} 0 & \text{for } \langle\theta_j\rangle = 0 \text{ or } \langle\theta_{j'}\rangle = 1 \\ \dfrac{\Delta_{j\to j'}}{Y\langle\theta_j\rangle(1-\langle\theta_{j'}\rangle)} & \text{for } \langle\theta_j\rangle \neq 0 \text{ and } \langle\theta_{j'}\rangle \neq 1 \end{cases} \tag{7}$$

As shown in Figure 5, the most probable displacements are for moving $\pm 1$ layer, thereby giving credit to the diffusive description of ion-induced particle relocation employed in the original reference.[6] The maximum number of displaced atoms from one layer to another is about three times larger than the maximum sputtering yield for any one layer. Therefore, the process of atomic relocation/mixing dominates over sputtering as far as the number of atomic movements is concerned. This observation does depend, however, on the beam conditions. As is shown later, for a beam polar angle of incidence of 70°, the maximum number of displaced atoms relative to the maximum number of sputtered atoms is almost comparable.

**Extracting Depth Profiles.** The solution to the differential equations, eq 2, gives the filling factor of the space fixed layers as a function of the amount of monolayer equivalents removed $x$. What is needed, however, is the depth profile of an *original* layer. As explained in the Krantzman and Wucher paper,[6] this is accomplished by considering the system to be comprised of $N$ subsystems where each subsystem tracks the evolution of the particles in one initial layer. Therefore, the subsystems each start with only one layer occupied with the initial filling factor. Each subsystem is integrated according to eq 2, and the particles from each initial layer become distributed among other layers within respective subsystems. Thus, the fate of particles originating from


dx.doi.org/10.1021/jp2098075 |J. Phys. Chem. C 2012, 116, 1042–1051

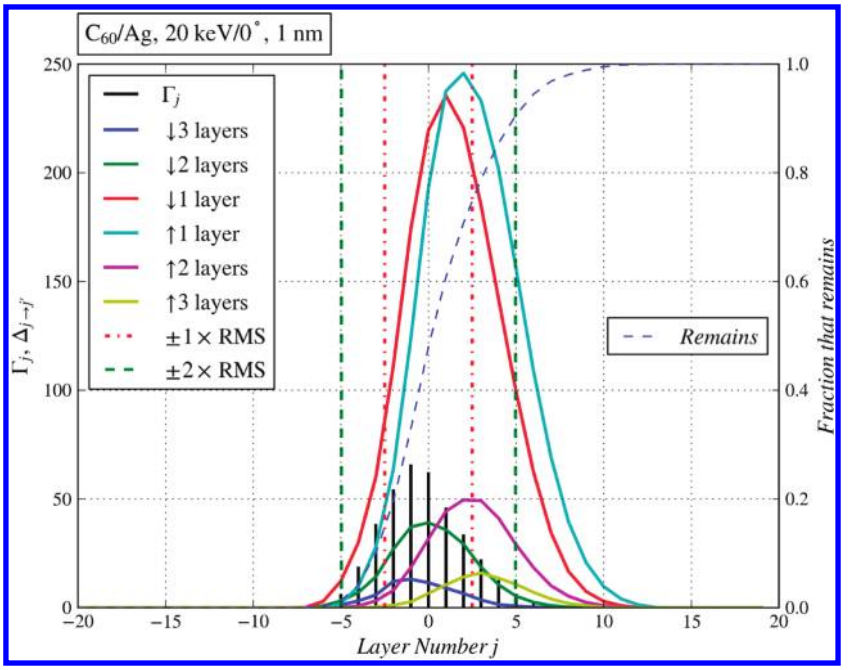


**Figure 5.** Average number of sputtered particles per layer, $\Gamma_j$, and average number of displaced particles per layer, $\Delta_{j\rightarrow j'}$, vs layer number, $j$. The sputtering yields are shown as vertical lines whereas the displacement yields are smooth lines with the color code defined in the legend. The red and green vertical lines correspond to $\pm 1$ and $\pm 2$ × rms roughness positions, respectively. The dashed blue line gives the fraction of a layer that remains in the layer, that is, is neither sputtered nor displaced.

each initial layer is tracked throughout the SS-SSM calculation. There are, in essence, $N^2$ filling factors followed in the calculation. Each filling factor is labeled by the initial layer that was occupied and the current layer. Thus, one can easily obtain the distribution of particles that were in, for example, the 14th initial layer. Alternatively, one can determine the number of particles, for example, in the current 14th layer by summing the respective filling factors from all of the subsystems. This coupling of the subsystems is utilized to calculate the total depth distribution of particles required at each step of integration to determine the average surface level, that is, the level with the filling factor closest to 0.5.

The computational effort of the SS-SSM is modest. Depending on the width of the $\Gamma$ and $\Delta$ distributions shown in Figure 5, the amount of CPU time to calculate a depth profile is between a few hours and a day. This time is small compared to the months it takes to perform a depth profiling MD simulation.

## DEPENDENCE ON MODEL QUANTITIES

The MD results in the steady-state region remove approximately two monolayer equivalents of material; thus, the comparison between the MD simulation and the SS-SSM that can be made is the evolution of the layer filling as a function of surface erosion as shown in Figure 6. Overall, the curves obtained by solving eq 2 and the curves obtained directly from MD simulations exhibit similar trends. Overall, we feel that the agreement is sufficient to use the SS-SSM to interpret the importance of various quantities such as the depth distribution of sputtered atoms (information depth) and the amount of displacements between layers on the depth profiles. As a check of the model, we calculated the filling factors as a function of the number of monolayers removed. The filling factor distribution remains the same as the initial one shown in Figure 3.

Depth profiles are calculated as the negative of the derivative of the fraction of particles from an initial layer that remains in the system. For all layers that are initially fully occupied, the fraction of particles that remains in the system has a characteristic sigmoidal shape starting at a value of one (fully occupied layer) and going to zero (fully unoccupied). A depth profile for the layer that is initially 14 layers below the original average surface level is shown as green dots in Figure 7. This layer is located approximately 14 nm below the original average surface level. The curves of the fraction of particles that remains in the system (not shown) are continuous but not smooth due to the index shifting when each monolayer equivalent is eroded; thus, the depth profile has jumps. In addition, the curvature of each segment does not perfectly match the overall curvature of the function. Thus, the curvature of the individual segments switches before the maximum of the depth profile. Since the depth profile corresponds to the removal of one monolayer, the integral of the depth profile distribution should be unity, which it is, even with the jaggedness of the profile. Since as mentioned in the next paragraph, the depth profiles fit well to a functional form preserving the amount of material removed, we do not feel it is necessary to smooth the curves of the fraction of particles that remains in the solid so that the derivative looks nice.

Experimentally the depth profiles are typically fit to the Dowsett analytical response function (ARF).[7] Following others,[8,9] we write it as

$$\mathrm{ARF}(x) = N\left[(1-\mathrm{erf}(\xi_1))\ \exp\left(\frac{x-x_0}{\lambda_g}+\frac{\sigma^2}{2\lambda_g{}^2}\right) + (1+\mathrm{erf}(\xi_2))\ \exp\left(-\frac{x-x_0}{\lambda_d}+\frac{\sigma^2}{2\lambda_d{}^2}\right)\right] \quad (8)$$


dx.doi.org/10.1021/jp2098075 |J. Phys. Chem. C 2012, 116, 1042–1051

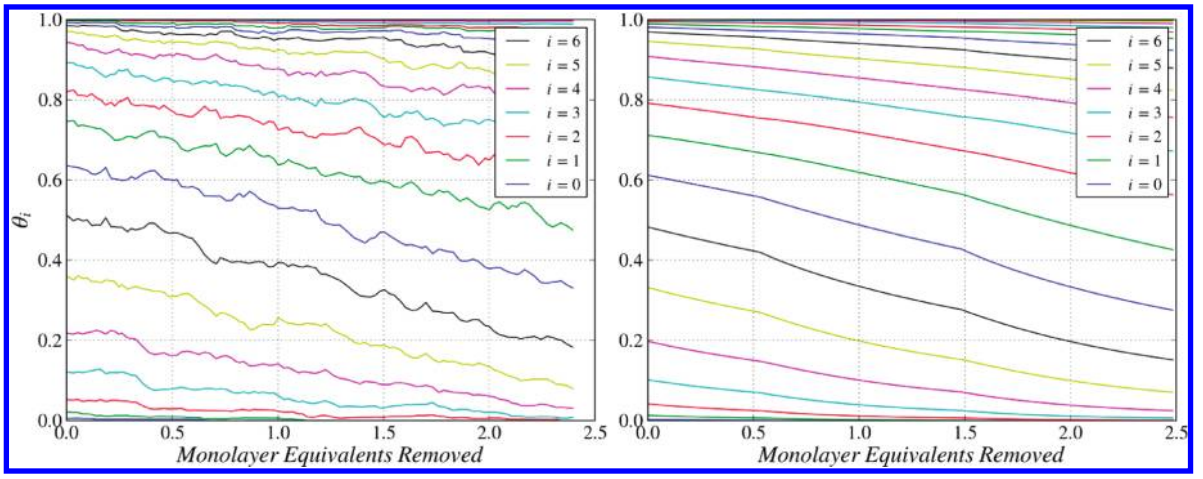


**Figure 6.** Layer filling, $\theta_i$, versus monolayer equivalents removed for several values of $i$ as shown in the legend. Left panel: MD simulations. Right panel: SS-SSM.

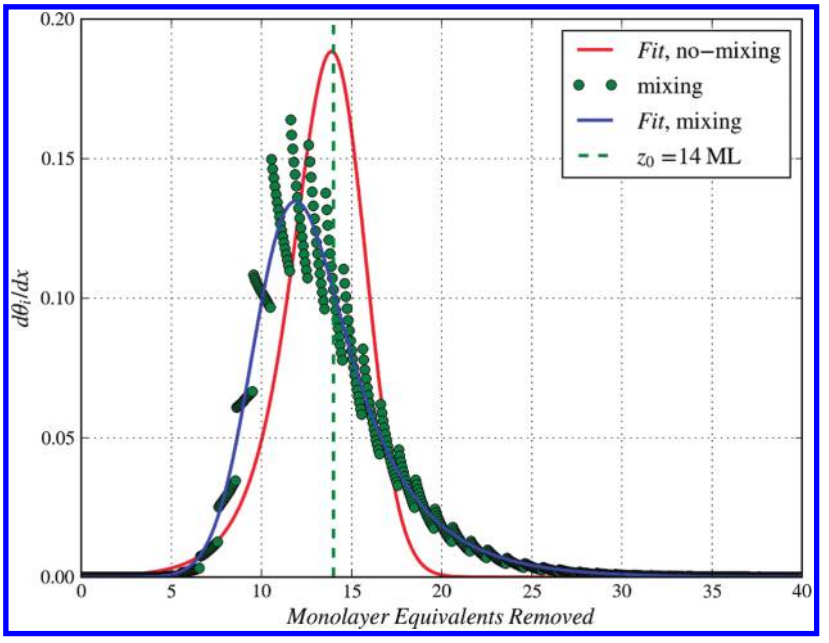


**Figure 7.** Depth profiles from SS-SSM vs monolayer equivalents removed. Green dots are directly from solution of eq 2. The blue line is the Dowsett ARF fit to the results from the SS-SSM with all mixing among layers. The red line is the Dowsett ARF fit to the results from the SS-SSM with no mixing among layers. The vertical green dashed line is the position, $z_0$, of the delta layer.

with

$$\xi_1 = \frac{1}{\sqrt{2}}\left(\frac{x - x_0}{\sigma} + \frac{\sigma}{\lambda_g}\right) \quad \text{and}$$

$$\xi_2 = \frac{1}{\sqrt{2}}\left(\frac{x - x_0}{\sigma} - \frac{\sigma}{\lambda_d}\right) \tag{9}$$

where $x_0$ is the peak position or apparent delta-layer position, $\lambda_g$ is the leading edge growth length, $\lambda_d$ is the trailing edge decay length, and $\sigma$ is the width of the central Gaussian connecting the growth and trailing edges. Shown in Figure 7 is the fit of the ARF to the results from the SS-SSM. The fitted function follows the results of the SS-SSM, maintaining a value of the integral of the ARF of unity. Since we are focusing on the qualitative nature of how the $C$ and $D$ distributions influence the depth profiles, we will not present the values of the fitted parameters of the ARF.

The first check of the model capabilities is to determine the effect of mixing on the depth profile.[6] The depth profile with no mixing, that is, with all $D_{j\to j'}$ set to zero, is shown in Figure 7. This distribution is almost centered at the delta layer position as expected. The inclusion of mixing shifts the peak position to an apparent higher position in the solid, the leading edge rises more quickly, and the trailing edge decays more slowly.[10,11] The width of the distribution is, however, not much changed, which indicates a minor influence of the mixing on this parameter, as compared to the effect it has on an ARF peak position.

At this point, we should, however, discuss an influence of the choice of layer thickness on the predictions of our model. The layer thickness was varied from 0.47 (two atomic Ag(111) layers) to 4.72 nm as shown in Figure 8. The rms roughness for this


dx.doi.org/10.1021/jp2098075 |J. Phys. Chem. C 2012, 116, 1042–1051

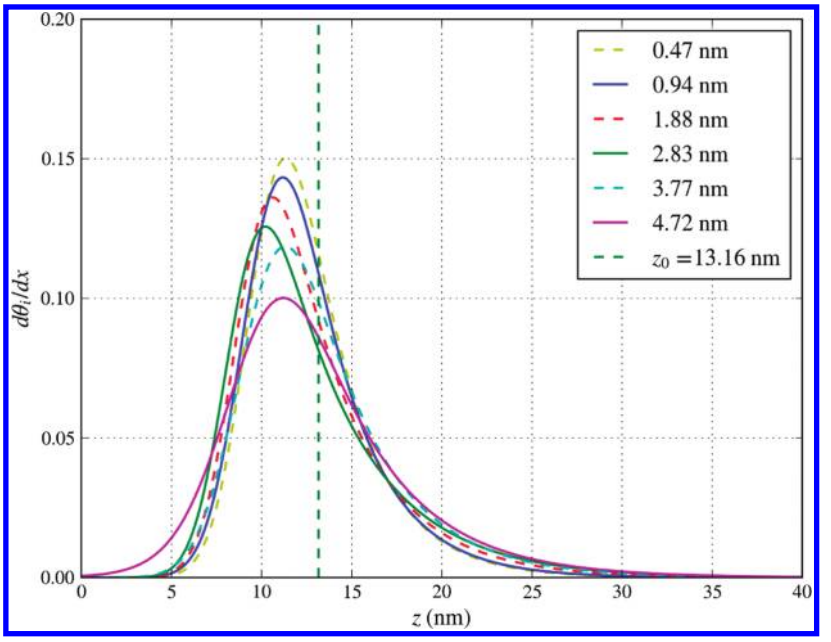


**Figure 8.** Depth profiles as a function of depth for various layer thicknesses as described in the legend.

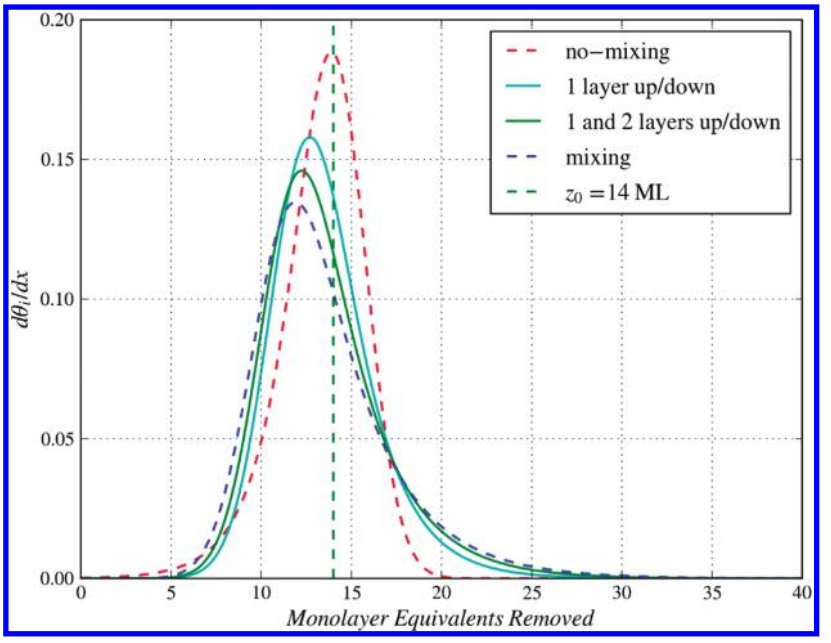


**Figure 9.** Depth profiles as a function of monolayer equivalents removed for different amounts of mixing included as described in the legend.

system is 2.35 nm, so three chosen layer thicknesses are less and three are larger than the rms roughness. Of note is that the *C* and *D* parameters have to be recalculated for each choice of layer thickness. In addition, the delta layer thickness is the same as the chosen layer thickness in the model. Overall, the depth profiles are remarkably independent of the choice of layer thickness up to about the value of the rms roughness. Naturally, the distribution broadens as the layer (and delta layer) thickness increases. From the point of view of spatial resolution, it is desirable to select thin layers although the computational resolution does not need to be smaller than that obtained experimentally. Our intuitive sense, however, is that larger layers are desirable as there will be fewer values of *C* and *D* and perhaps they it will be easier to understand the relationship between the bombardment event and the parameters. We choose to use the 0.94 nm (four atomic Ag(111) layers) layer thicknesses in the remainder of this study because it can be easily interpreted as 1 nm. Thus, the remainder of the depth profiles will be shown as a function of monolayer equivalents removed *x* which, when converted to depth, is approximately the same value in nanometers.

While mixing has a small influence on the depth profile width, it has a pronounced effect on its position as shown in Figure 7. Thus, next we investigate how the width of the mixing distribution will influence depth profiles. The effect of selectively keeping various interlayer displacement terms is shown in Figure 9. The original depth profiles with and without mixing from Figure 7 are

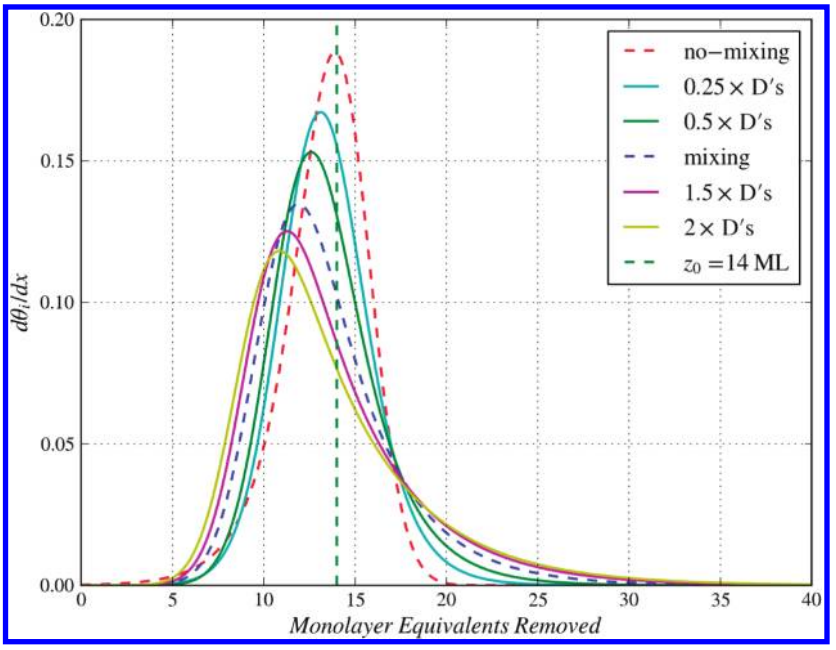


**Figure 10.** Depth profiles as a function of monolayer equivalents removed for different amounts of mixing included as described in the legend.

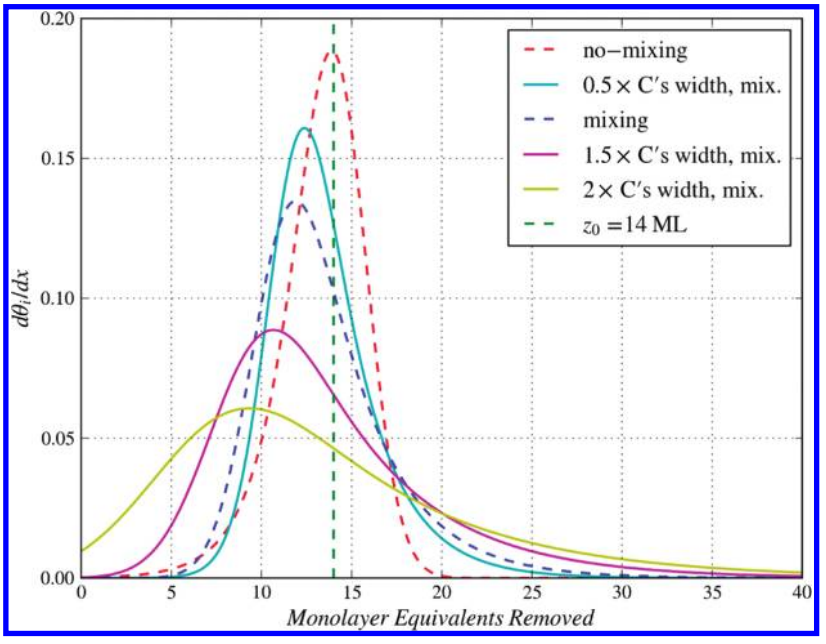


**Figure 11.** Depth profiles as a function of monolayer equivalents removed for different distributions of sputtering as described in the legend.

repeated. Keeping only the terms for particles moving up or down one layer accounts for about half of the shift in the depth profile from no-mixing to the full-mixing result.

The effect of relative contributions of sputtering and displacements is shown in Figure 10. The height of the *D* distribution was varied from a factor of 4 smaller, which makes the largest value of *D* about the same as the largest value of *C*, to a factor of 2 larger than the values shown in Figure 5. It is clear that the larger the amount of mixing, the greater the shift in the apparent delta layer position and the more asymmetric the depth distributions become. It seems, however, that most of this asymmetry is caused by an increase of the trailing edge decay length.[10,11] The rising edge decay length is less altered.

The artificial adjustments to the *C* distribution were also performed with the constraint that the condition described by eq 6 must be fulfilled. In other words, the width of the sputtering distribution, as shown in Figure 5, was varied from a factor of 2 smaller, which makes it comparable to $(-2 \div +1) \times$ rms roughness distance, to a factor of 2 larger, which makes it comparable to $(-2 \div +4) \times$ rms roughness distance. The results of these changes are shown in Figure 11. What is apparent is that the width of the *C* distribution affects all parameters of the Dowsett's ARF. The width of the depth profile is altered the most, while its position is less influenced. The words that are often used with the Dowsett ARF is that the width of the sputtering


dx.doi.org/10.1021/jp2098075 |*J. Phys. Chem. C* 2012, 116, 1042–1051

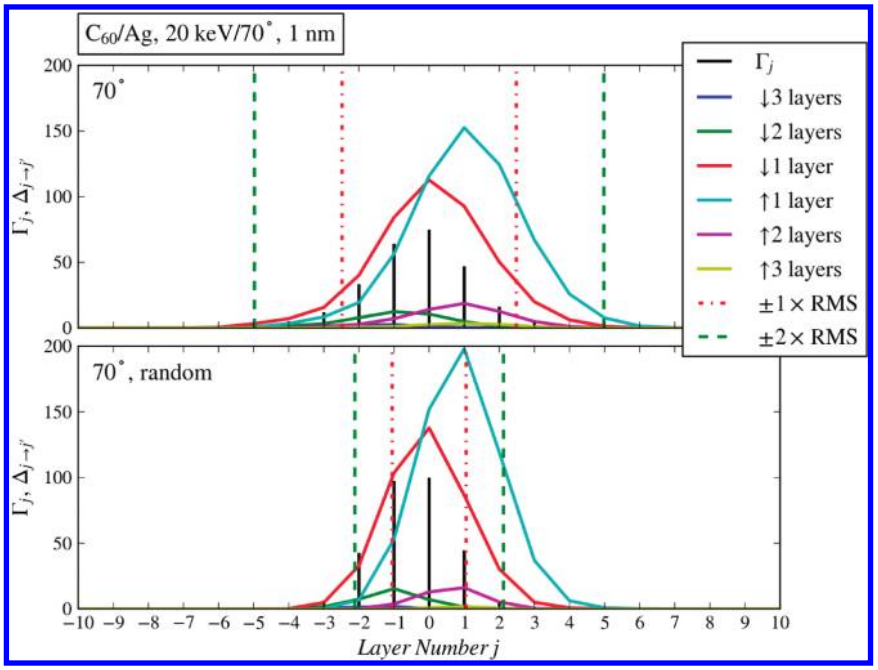


**Figure 12.** Average sputtering fraction, $\Gamma_j$, and average displacement fractions, $\Delta_{j\rightarrow j'}$, vs layer number, $j$, for the simulation with $C_{60}$ at 20 keV bombarding at 70° for a single azimuthal angle of incidence and random azimuthal angles of incidence.

distribution is a measure of the information depth which corresponds to the leading edge growth length. Our calculations do not support this vision as the shape of the sputtering information depth influences all of the parameters.

## INTERPRETATION OF EXPERIMENTAL RESULTS

Two examples of applying the SS-SSM to interpret real experimental data are chosen. The first is the depth resolution for $C_{60}$ bombardment of a Ni:Cr multilayer structure,[12,13] and the second is the effect of sample rotation on depth resolution.[14−16] In the first case, a direct comparison of depth resolution values is made. In the second case, a qualitative comparison is discussed.

The missing connection between the simulations and experiment is the relationship of the properties of material removal and the depth profile width. The MD simulations of dynamic SIMS show that the rms roughness is of the same size as the crater depths.[4,17] From Figure 3 it is clear that the roughened surface has a total height of 4 × rms roughness. The sputtering arises from the entire exposed region as shown in Figure 5; thus, the final depth profile full width at half-maximum (fwhm) of 7 nm as shown in Figure 7 reflects the roughness (the information depth of the sputtered material) and not directly the individual crater depth or the mixing.[4] It would be nice to be able to make a more direct connection between the characteristics of the individual craters and the depth profile width. This task is, however, one of the objectives in future studies with the SS-SSM. For comparison, experimentally a Ni:Cr multilayer structure has been depth-profiled using 10−20 keV $C_{60}$ bombardment.[12,13] It has been found that the depth resolution as determined from the first interface width varies from 5 to 8.7 nm over this energy range. This range of values is in excellent agreement with the value from the SS-SSM.

Recently experiments have been performed showing that sample rotation improves the quality of a depth profile for organic[14,16] and polymeric materials.[14] A MD study[15] was made in order to understand this effect. These same data sets[15] are analyzed with the SS-SSM. The $\Gamma_j$ and $\Delta_{j-j}$ values are shown in Figure 12 for 20 keV $C_{60}$ bombardment of Ag(111) at 70° incidence for a single angle of incidence and for a random angle of incidence (computational equivalent of sample rotation). The corresponding depth profiles are shown in Figure 13. There are several observations. (1) Sputtering distributions are narrower from the set of conditions discussed above. The largest sputtering yield is for the $j = 0$ layer, the average surface level, a one layer difference. (2) The largest number of displacements are again for moving ±1 layer but, in contrast to the model system discussed above, the maximum number of displaced atoms is only slightly larger than the maximum sputtering yield for any layer. This condition suggests that off-normal angles of incidence should be better than normal incidence for depth profiling (narrower ARF which peaks closer to the real position of a delta-layer), a condition observed in experiments[18−20] and in simulations.[21,22] (3) The width of the sputtering distribution with a random azimuthal angle of incidence is smaller than for a single azimuthal incidence because the rms roughness is smaller for the random azimuth simulations. (4) The yield as indicated by the sum of the vertical bars of the C distribution is larger with a random azimuthal angle of incidence. The obvious conclusion from Figure 13 is that the depth profile with sample rotation (random azimuthal direction) is narrower and has the peak position closer to the Δ layer because the rms roughness is smaller. Thus, the simulations are in agreement with experiment that sample rotation will give better depth profiles than without sample rotation. This conclusion was reached both by examining just the rms roughness[15] and by using the SS-SSM to predict depth profiles. It should be emphasized, however, that the SS-SSM does not provide the mechanistic reason of why sample rotation helps. That information must come from pictures and concepts gleaned from the microscopic MD simulations.[15]

## SUMMARY

The statistical sputtering model of Krantzman and Wucher provides a formalism for utilizing information from molecular

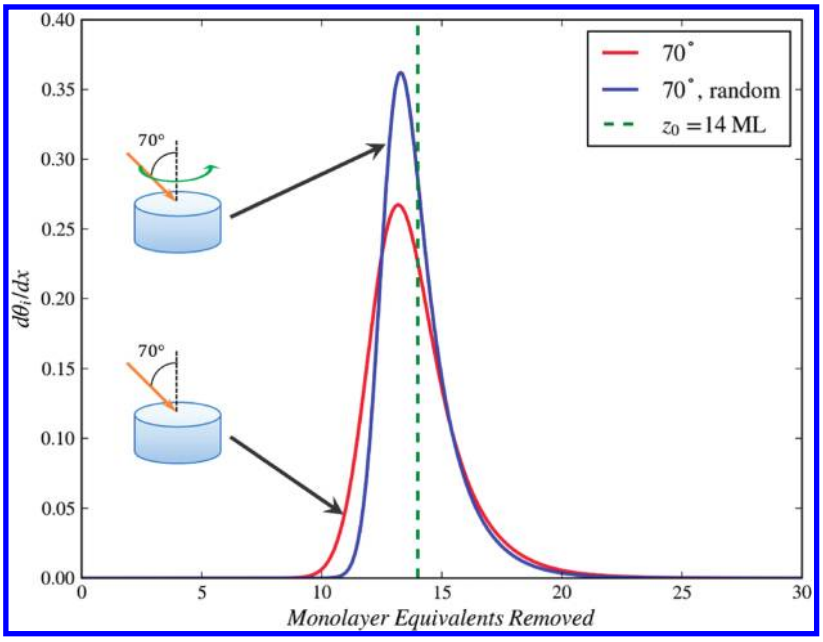


**Figure 13.** Depth profiles vs monolayer equivalents removed for a single and random azimuthal angles of incidence.

dynamics simulations of dynamic SIMS and extracting depth profiles. This model has been modified to utilize parameters extracted from the steady-state region of the molecular dynamics simulations and to include explicit displacement contributions between all pairs of layers. The SS-SSM has been applied to results of a simulation of 20 keV $C_{60}$ bombardment of a Ag(111) surface to estimate the relative contribution of the sputtering and atomic mixing into the modification of eroded sample. The model allows identification of the influence of the sputtering information depth and the atomic mixing on the depth profiles. The results show that the greater the number of displacements to adjacent layers (mixing) relative to the number of sputtered particles per layer the greater the shift in the apparent delta layer position relative to the actual position. The greater the width of the distribution of the number of sputtered particles per layer, that is, the information depth, the larger the width of the delta layer profile. The SS-SSM will be used in the future to analyze the data from MD simulations of dynamic SIMS by a number of different clusters with different beam conditions in order to connect the microscopic details of the bombardment events with the depth profiles. In addition, the model will be developed further to include both intact molecules and chemically damage molecules. In conjunction with planned MD simulations of molecular depth profiling, we anticipate that this SS-SSM will be a platform for understanding the importance of chemical damage on molecular depth profiling.

## AUTHOR INFORMATION

### Corresponding Author

*E-mail: bjg@psu.edu.

## ACKNOWLEDGMENT

We gratefully acknowledge financial support from the National Science Foundation Grant No. CHE-0910564 and the Polish Ministry of Science and Higher Education Programs No. PB1839/B/H03/2011/40. We are extremely grateful to Kristin Krantzman for helpful discussions and insight into the original SSM.

## REFERENCES

(1) Winograd, N. *Anal. Chem.* **2005**, *77*, 142A–149A.
(2) Russo, M. F.; Postawa, Z.; Garrison, B. J. *J. Phys. Chem. C* **2009**, *113*, 3270–3276.
(3) Paruch, R.; Rzeznik, L.; Russo, M. F.; Garrison, B. J.; Postawa, Z. *J. Phys. Chem. C* **2010**, *114*, 5532–5539.
(4) Postawa, Z.; Rzeznik, L.; Paruch, R.; Russo, M. F.; Winograd, N.; Garrison, B. J. *Surf. Interface Anal.* **2011**, *43*, 12–15.
(5) Rzeznik, L.; Paruch, R.; Garrison, B. J.; Postawa, Z. *Nucl. Instrum. Methods Phys. Res., Sect. B* **2011**, *269*, 1586–1590.
(6) Krantzman, K. D.; Wucher, A. *J. Phys. Chem. C* **2010**, *114*, 5480–5490.
(7) Dowsett, M. G.; Rowlands, G.; Allen, P. N.; Barlow, R. D. *Surf. Interface Anal.* **1994**, *21*, 310–315.
(8) Homma, Y. *J. Vac. Soc. Jpn.* **2005**, *48*, 265–269.
(9) Lu, C. Y.; Wucher, A.; Winograd, N. *Anal. Chem.* **2011**, *83*, 351–358.
(10) Liau, Z. L.; Tsaur, B. Y.; Mayer, J. W. *J. Vac. Sci. Technol.* **1979**, *16*, 121–127.
(11) Zalm, P. C. *Mikrochim. Acta* **2000**, *132*, 243–257.
(12) Sun, S.; Wucher, A.; Szakal, C.; Winograd, N. *Appl. Phys. Lett.* **2004**, *84*, 5177–5179.
(13) Sun, S.; Szakal, C.; Roll, T.; Mazarov, P.; Wucher, A.; Winograd, N. *Surf. Interface Anal.* **2004**, *36*, 1367–1372.
(14) Bryan, S. R. Unpublished information, 2011.
(15) Garrison, B. J.; Postawa, Z. *Chem. Phys. Lett.* **2011**, *506*, 129–134.
(16) Sjovall, P.; Rading, D.; Ray, S.; Yang, L.; Shard, A. G. *J. Phys. Chem. B* **2010**, *114*, 769–774.
(17) Aoki, T.; Seki, T.; Matsuo, J. *Vacuum* **2010**, *84*, 994–998.
(18) Kozole, J.; Wucher, A.; Winograd, M. *Anal. Chem.* **2008**, *80*, 5293–5301.
(19) Kozole, J.; Willingham, D.; Winograd, N. *Appl. Surf. Sci.* **2008**, *255*, 1068–1070.
(20) Rading, D.; Moellers, R.; Kollmer, F.; Paul, W.; Niehuis, E. *Surf. Interface Anal.* **2011**, *43*, 198.
(21) Ryan, K. E.; Garrison, B. J. *Anal. Chem.* **2008**, *80*, 5302.
(22) Ryan, K. E.; Smiley, E. J.; Winograd, N.; Garrison, B. J. *Appl. Surf. Sci.* **2008**, *255*, 844.